J Adv Ceram

Research Article

Tribocatalytic activation of peroxymonosulfate by TiO_2 nanoparticles for powerful degradation of organic pollutants

Zeren Zhou[1], Ruijiang Chen[2], Hanze Zhu[1], Yongming Hu[3], Najun Li[2], Wanping Chen[1,✉]

Cite this article: Zhou Z, Chen R, Zhu H, et al. *J Adv Ceram* 2026, **15**(2): 9221237. https://doi.org/10.26599/JAC.2025.9221237

ABSTRACT: Sulfate radical ($SO_4^{\cdot-}$)-based advanced oxidation processes have received increasing interest for the treatment of organic wastewater, and various methods are being intensively investigated to activate peroxydisulfate (PDS) or peroxymonosulfate (PMS) to generate $SO_4^{\cdot-}$. Presently, we have explored the activation of PMS via tribocatalysis for the first time. In glass beakers with polytetrafluoroethylene (PTFE) disks coated on the bottoms, solutions of organic pollutants suspended with TiO_2 nanoparticles were subjected to magnetic stirring to realize tribocatalytic degradation. To our great surprise, the addition of 200 mg/L PMS was found to greatly enhance the tribocatalytic degradation of 50 mg/L rhodamine B (RhB), methylene blue (MB), and methyl orange (MO) solutions and 20 mg/L bisphenol A (BPA) and phenol solutions, which were all degraded rather thoroughly in quite short periods of time, and their total organic carbon removals were substantially improved. Electron paramagnetic resonance spectroscopy analyses showed that the addition of PMS not only led to the formation of $SO_4^{\cdot-}$ but also dramatically increased the amount of ·OH, $O_2^{\cdot-}$, and $^1O_2$ when TiO_2 nanoparticles were stimulated through magnetic stirring. It is proposed that electron–hole pairs are excited in TiO_2 nanoparticles by mechanical energy absorbed through friction, which react with PMS to generate $SO_4^{\cdot-}$ and other radicals. These findings demonstrate an energy-efficient paradigm for PMS activation, and many more studies on tribocatalytic activation of PDS/PMS are highly desirable.

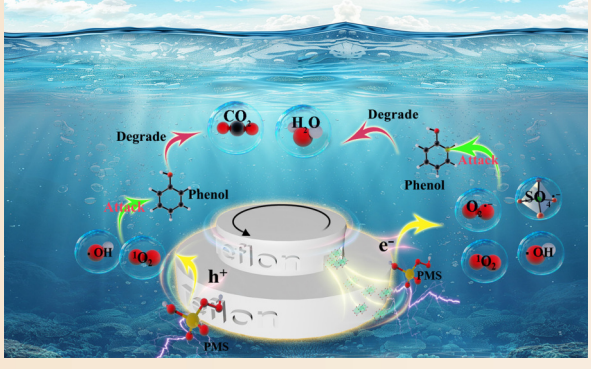

KEYWORDS: tribocatalysis; dye degradation; wastewater; peroxymonosulfate; TiO_2

1 Introduction

With the rapid progression of industrialization and urbanization, organic contaminants in the aquatic environment have aroused growing concern worldwide [1]. Many of them, such as organic dyes and phenolic compounds, not only possess pronounced toxicity and carcinogenicity but also exhibit high chemical stability and structural complexity [2,3]. For their treatment, conventional wastewater treatment techniques, including physical adsorption, coagulation-precipitation, and biological treatments, suffer from shortcomings such as slow reaction kinetics, incomplete degradation, and/or the risk of secondary pollution. On the other hand, advanced oxidation processes (AOPs) that are based on the *in situ* generation of active free-radical species have been particularly developed for eliminating recalcitrant organic contaminants [4–7]. H_2O_2, O_3, persulfates, and chlorine are well-known radical promoters in AOPs, which can be conveniently activated through ultraviolet (UV) irradiation to generate active free-radical species such as ·OH, $O_2^{\cdot-}$, $^1O_2$, $SO_4^{\cdot-}$, and Cl· [1,8–10]. UV/H_2O_2 and UV/Cl_2 have found full-scale applications for potable water reuse [11]. However, due to the limited penetration of UV in wastewater, UV/radical promoters are not established for advanced wastewater treatment.

·OH is the most common free radical in various AOPs [12]. As $SO_4^{\cdot-}$ has a longer half-life span (30–40 μs) and a higher redox potential in a broader pH range than ·OH, whose half-life span is only approximately 20 ns, sulfate radical-based AOPs have received increasing attention in recent years [13–16]. Aimed at advanced wastewater treatment, peroxymonosulfate (PMS) and peroxydisulfate (PDS) are being intensively explored to generate $SO_4^{\cdot-}$ through activation processes other than UV irradiation. It is well-known that mechanical energy is a clean energy widely available in the ambient environment. In this context, ultrasound has been successfully implemented to activate PMS in the presence of some piezoelectric nanomaterials in several studies, where the piezoelectric nanomaterials suspended in water were

[1] School of Physics and Technology, Wuhan University, Wuhan 430072, China. [2] College of Chemistry, Chemical Engineering and Materials Science, Soochow University, Suzhou 215123, China. [3] Hubei Key Laboratory of Micro-Nanoelectronic Materials and Devices, School of Intelligent Manufacturing, Hubei University, Wuhan 430062, China.

✉ Corresponding author. E-mail: wpchen@whu.edu.cn

Received: September 12, 2025; Revised: December 27, 2025; Accepted: December 27, 2025

deformed to generate electricity through ultrasound, which in turn activated PMS to degrade organic pollutants [17]. This is actually a typical piezocatalytic process, and piezocatalytic activation of PMS has been studied for the degradation of benzothiazole [18], antibiotic ornidazole [19], ibuprofen, and phenol [20]. Obviously, similar to UV irradiation, ultrasound can be conveniently input from outside to activate PMS as well as PDS. However, the application of ultrasound to activate PMS/PDS is too energy intensive for large-scale wastewater treatment [21], which underscores a need to develop mechanical energy-based PMS/PDS activation strategies that are more energy efficient and more energy conserving.

In fact, tribocatalysis has emerged as another form of mechanocatalysis in addition to piezocatalysis in recent years [22–24]. Usually, driven through magnetic stirring, tribocatalysis converts mechanical energy directly into chemical energy through mechanical friction and is characterized by advantages of low energy consumption, high efficiency, and excellent environmental adaptability, particularly under ambient temperature and dark conditions [25,26]. Presently, we have explored the tribocatalytic activation of PMS using TiO_2 nanoparticles as the tribocatalyst. To our great surprise, some typical organic pollutants that have been rather time-consuming or even impossible to degrade through tribocatalysis alone [27], including relatively high-concentration rhodamine B (RhB), methylene blue (MB), methyl orange (MO), and phenolic contaminants of phenol and bisphenol A (BPA), have all been rather thoroughly degraded in relatively short periods of time through the combination of tribocatalysis and PMS. The low transparency of organic pollutant solutions is a great challenge to their photocatalytic treatment [28], while tribocatalysis is employed to degrade organic dyes at increasing concentrations [27,29], which suggests that tribocatalysis has an advantage over photocatalysis in treating wastewater of low transparency. Now, with a great acceleration in tribocatalytic degradation speed obtained through the addition of PMS in this study, we believe that the findings in this study open a new frontier in PMS-based advanced oxidation, especially for treating wastewater with low transparency.

2 Experimental

2.1 Materials and characterizations

The TiO_2 nanoparticles used in this study were purchased from Shanghai Macklin Biochemical Technology Co., Ltd., China. X-ray diffraction (XRD) patterns were collected using a diffractometer (BRUKER AXS D8 ADVANCE, Germany) equipped with Cu Kα radiation (λ = 1.54056 Å). The microstructure of the TiO_2 nanoparticles was further examined by a high-resolution transmission electron microscope (HRTEM; Tecnai G2 F30, FEI, USA). A specific surface area and porosity analyzer (ASAP 2460, Micromeritics, USA) was used to determine and calculate the specific surface area of the TiO_2 nanoparticles with the Brunauer–Emmett–Teller (BET) equation.

2.2 Degradation experiments of organic pollutant solutions

A polytetrafluoroethylene (PTFE) disk (diameter: 40 mm; thickness: 1 mm) was firmly affixed to the bottom of a commercial flat-bottom glass beaker (ϕ40 mm × 60 mm) using a strong adhesive. In this way, glass beakers with PTFE coatings on their bottoms were used in subsequent experiments. The tribicatalytic degradation of 100 mg/L MO by $BaTiO_3$ nanoparticles was recently reported to be much faster in beakers with PTFE coatings than with Ti, Al_2O_3 coatings, and glass bottoms [27].

The solutions of organic pollutants were divided into two groups for comparison. In group 1, the solutions were 50 mg/L RhB, 50 mg/L MB, 50 mg/L MO, 20 mg/L BPA, and 20 mg/L phenol. In group 2, these five kinds of solutions were all supplemented with 200 mg/L PMS.

In a typical degradation experiment, 0.30 g of TiO_2 nanoparticles was dispersed in 30 mL of an organic pollutant solution in a PTFE-coated beaker. A homemade PTFE magnetic rotary disk, which was described in detail in a previous study [30], was placed in the suspension and was driven to rotate at 400 r/min. There was a cross-shaped groove in the surface of the PTFE magnetic rotary disk, which facilitated TiO_2 nanoparticles to reach the interface between the rotary disk and the beaker bottom in the course of magnetic stirring. The entire process was carried out in the dark at room temperature (25 °C). At designated intervals, 2 mL of the suspension was withdrawn and treated through centrifugation at 8000 r/min for 5 min to remove suspended TiO_2. For the PMS-containing solutions, 1 mL of methanol was added before centrifugation to quench any residual PMS. The absorbance spectra of the resulting supernatants were recorded using a UV–visible (UV–Vis) spectrophotometer (UV-2550; Shimadzu, Japan). Every degradation experiment was repeated at least three times, and only the results obtained from representative experiments were adopted.

Total organic carbon (TOC) measurement is widely used to examine genuine mineralization in the degradation of organic pollutants [31]. In this study, the TOC of PMS-free and PMS-supplemented solutions after 1 h of magnetic stirring was quantified using a TOC analyzer (Multi N/C 3100, Analytik Jena, Germany).

2.3 Active species analyses

For the detection of ·OH and $SO_4^{\cdot-}$, 10.0 mL of deionized water and 2 mg of PMS were added to a glass beaker (φ40 mm × 60 mm) with PTFE coating, and 0.05 mL of 5,5-dimethyl-1-pyrroline N-oxide (DMPO) was added as a trapping agent. For the detection of $^1O_2$, 10.0 mL of deionized water and 2 mg of PMS were added to a glass beaker with PTFE coating, and 0.05 mL TEMP was added as a trapping agent. For the detection of $O_2^{\cdot-}$, 9.0 mL methanol and 1.0 mL PMS aqueous solution (2 mg PMS dissolved in 1 mL deionized water) were added to a glass beaker with PTFE coating, and 0.05 mL DMPO was added as a trapping agent. All beakers were kept in the dark, 50 mg TiO_2 nanoparticles were added, and the suspensions were stirred at 400 r/min for 30 min at room temperature using a PTFE magnetic rotary disk. The resulting suspensions were analyzed using an electron paramagnetic resonance (EPR) spectrometer (Bruker EPR A300-10/12, Germany) to discern the presence of radicals. For comparison, three control experiments were conducted without PMS, while all the others under conditions were identical.

Free radical quenching experiments were performed in the course of tribocatalytic degradation of 50 mg/L MB with 200 mg/L PMS by TiO_2 nanoparticles. 500 mM tert-butanol (TBA; quenching ·OH), 50 mM furfuryl alcohol (FFA; quenching $^1O_2$), 500 mM methanol (MeOH; quenching both ·OH and $SO_4^{\cdot-}$), and 2 mM p-benzoquinone (p-BQ; quenching $\cdot O_2^-$) were used as scavengers separately.

3 Results and discussion

3.1 Materials information

The XRD pattern of the TiO_2 nanoparticles used in this study is

shown in Fig. 1(a). By comparing the observed diffraction peaks with those from the standard card of anatase TiO_2 (PDF#00-021-1272), all the main peaks could be indexed as crystal planes of anatase TiO_2, suggesting that the commercial TiO_2 powder is of the anatase phase with high purity. TEM image of the TiO_2 nanoparticles reveals that most grains have round granular shapes with particle sizes below 20 nm, as shown in Fig. 1(b). HRTEM image obtained for a TiO_2 nanoparticle, as presented in Fig. 1(c), clearly illustrates perfect lattice fringes across the whole nanoparticle. The lattice spacing was calculated to be 0.352 nm, which corresponds precisely to that of the (101) crystal plane of anatase TiO_2. Obviously, a high crystallinity was clearly revealed for the TiO_2 nanoparticles used in this study.

The N_2 adsorption–desorption isotherm at 77 K was measured for the TiO_2 nanoparticles, as shown in Fig. S1 in the Electronic Supplementary Material (ESM). The BET surface area of the TiO_2 nanoparticles was calculated to be 100.8 $m^2 \cdot g^{-1}$, which is consistent with the image shown in Fig. 1(b) regarding the size of the TiO_2 nanoparticles.

3.2 PMS-enhanced tribocatalytic degradation of organic pollutants by TiO_2 nanoparticles

First, it should be noted that TiO_2 nanoparticles have shown quite impressive tribocatalytic performance in degrading organic dyes with PTFE magnetic rotary disks used in magnetic stirring [32,33]. For the TiO_2 nanoparticles in this study, 50 mg/L RhB, MB, and MO were degraded by 90%, 30%, and 80%, respectively, after 3 h of magnetic stirring, as shown in Fig. 2. Generally, such results are very outstanding compared with those reported for tribocatalytic degradation of organic dyes in Refs. [34,35]. It is thus a great surprise to us that the tribocatalytic degradation of these three kinds of organic dye solutions was greatly enhanced through the addition of PMS: 50 mg/L RhB was degraded by 100% after only 1 h of magnetic stirring, 50 mg/L MB was degraded by 97.7% after 2 h of magnetic stirring, and 50 mg/L MO was degraded by 99.9% after 1 h of magnetic stirring. It is worth noting that a notable redshift could be observed for the MO solution in the course of its degradation, which has also been reported in some previous studies [33]. Obviously, PMS must have participated in and greatly improved the tribocatalytic degradation of the organic dyes by TiO_2 nanoparticles.

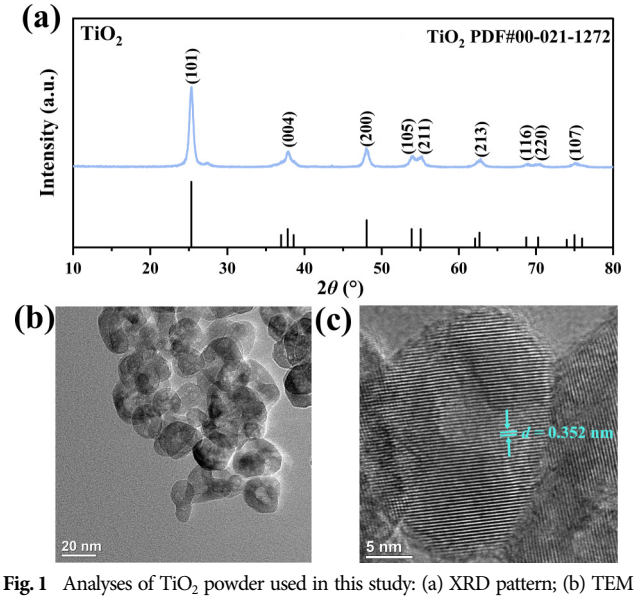

Fig. 1 Analyses of TiO_2 powder used in this study: (a) XRD pattern; (b) TEM image; (c) HRTEM image.

TiO_2 nanoparticles have been used repeatedly to degrade 50 mg/L MB with 200 mg/L PMS to evaluate their cyclic stability in the presence of PMS. As shown in Fig. S4(a) in the ESM, the degradation rate of MB remained as high as 97.6% after five consecutive cycles. No significant changes were observed in their morphology after these repeated uses, either, as shown in Fig. S4(b) in the ESM. These results indicate the excellent stability of the TiO_2 nanoparticles in the tribocatalytic degradation of organic pollutants in the presence of PMS.

In addition to organic dyes, another major group of organic pollutants in wastewater is various kinds of phenolic contaminants [36]. As BPA and phenol are two kinds of phenolic contaminants whose degradation is being intensively investigated in Ref. [37], they have also been chosen as model organic pollutants in this study. For 20 mg/L BPA, the peak at 275 nm gradually decreased in intensity with magnetic stirring time, and a 90% reduction was reached after 5 h of magnetic stirring, as shown in Fig. 3(a). For 20 mg/L BPA and 200 mg/L PMS, the degradation was dramatically accelerated. The peak at 275 nm decreased by 99.8% after only 1 h of magnetic stirring, as shown in Fig. 3(b).

Phenol is a well-known recalcitrant organic pollutant [38]. It is thus no surprise that for 20 mg/L phenol, its characteristic band remained essentially unchanged over 4 h of magnetic stirring, indicating that the tribocatalysis of TiO_2 alone was ineffective in degrading phenol, as shown in Fig. 3(c). In sharp contrast, for 20 mg/L phenol and 200 mg/L PMS, the band at 269–275 nm diminished rapidly in the course of magnetic stirring, as shown in Fig. 3(d). It is interesting to note that a transient peak at ~245 nm quickly appeared and then disappeared. After 5 h of magnetic stirring, the transient peak at ~245 nm completely disappeared, while the original peak at 270 nm was reduced by 90%. Obviously, PMS has played a vital role in the degradation of phenol [39].

It is worth emphasizing that PMS has significantly enhanced the tribocatalytic degradation by TiO_2 nanoparticles for all five common types of organic pollutants investigated in this study. To show more clearly, curves of C/C_0 (for a specific organic pollutant, the ratio of its remaining absorbance to initial absorbance at its characteristic peak in UV–Vis absorption spectra is generally adopted as the ratio of its remaining concentration to initial concentration, namely C/C_0) versus magnetic stirring time for tribocatalytic degradation of PMS-free and PMS-added RhB, MB, MO, BPA, and phenol solutions by TiO_2 nanoparticles were plotted in Fig. 4, and their pseudo-first-order rate constants were calculated and presented in Table 1. Compared to the PMS-free group, solutions in the PMS-supplemented group were degraded much more quickly by magnetic stirring-stimulated TiO_2 nanoparticles. The most remarkable enhancement was obtained for the degradation of phenol, whose pseudo-first-order rate constant was changed from 0 to 0.0064 min^{-1}. For the other four kinds of organic pollutants, the increase in the pseudo-first-order rate constant ranged from 2.6-fold for RhB to 9.4-fold for MB. These results suggest promising general validity for the combination of tribocatalysis and PMS.

TOC analyses further justified the combination of tribocatalysis and PMS. As shown in Fig. 5, 1-h TOC removal through tribocatalysis of TiO_2 nanoparticles alone was generally low for all five kinds of organic pollutant solutions: ~35% for RhB, less than 20% for MB, MO, and BPA, and negligible for phenol. In contrast, upon PMS addition, 1-h TOC removal was markedly increased for all five kinds of organic pollutant solutions: over 80% for RhB and MO, ~60% for MB, ~75% for BPA, and ~25% for phenol. As shown in Fig. 3(d), the transient peak at ~245 nm did not disappear even after 4 h of magnetic stirring in the course of degradation of phenol with PMS, which indicates the existence of

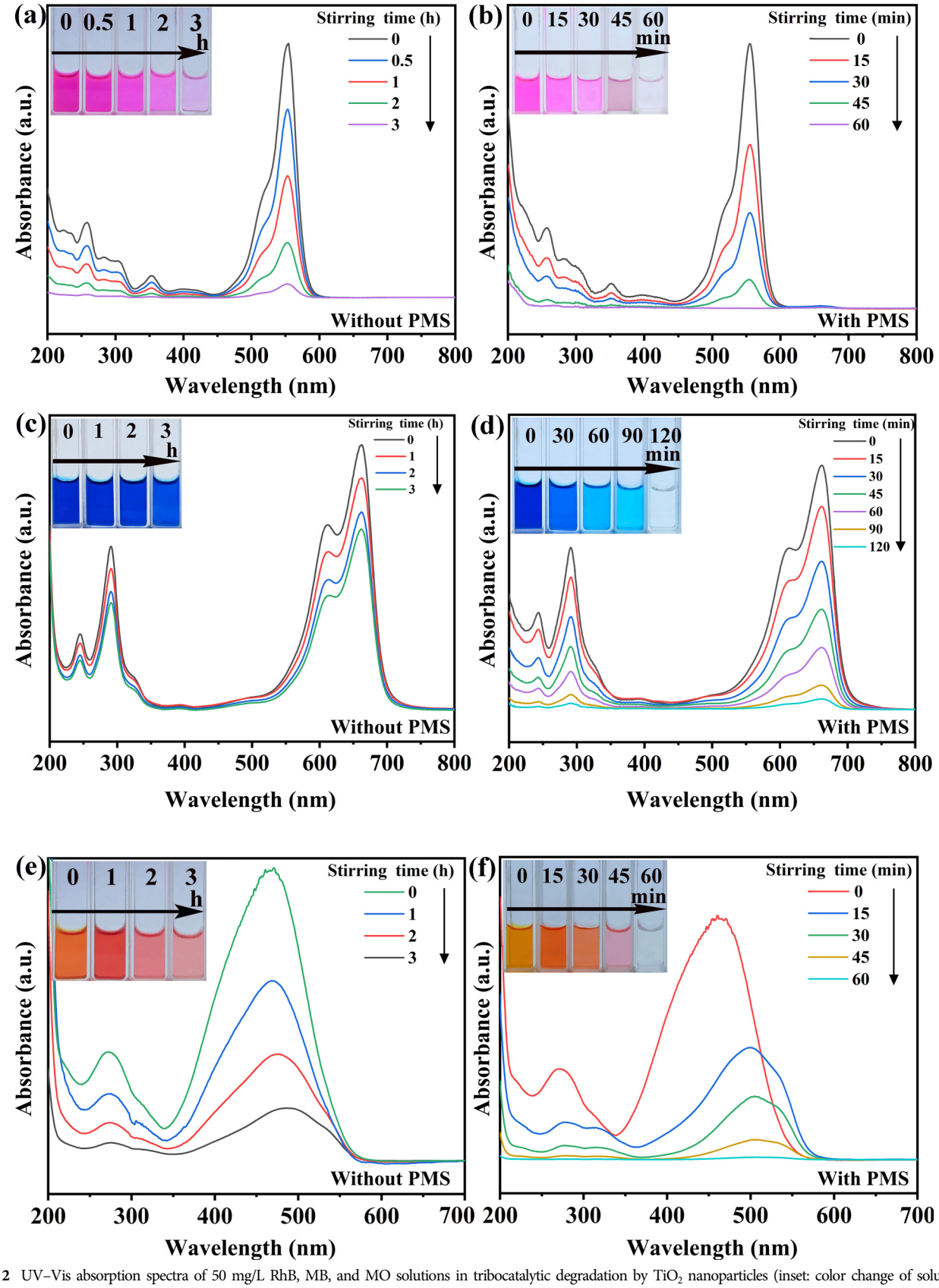

Fig. 2 UV–Vis absorption spectra of 50 mg/L RhB, MB, and MO solutions in tribocatalytic degradation by TiO_2 nanoparticles (inset: color change of solution). (a) 50 mg/L RhB; (b) 50 mg/L RhB and 200 mg/L PMS; (c) 50 mg/L MB; (d) 50 mg/L MB and 200 mg/L PMS; (e) 50 mg/L MO; (f) 50 mg/L MO and 200 mg/L PMS.

intermediates at 4 h and explains the rather small 1-h TOC for phenol with PMS in Fig. 5. In previous studies of tribocatalytic degradation of MO, a new peak at approximately 250 nm appeared in UV–Vis absorption spectra, and it was revealed that MO molecules had only been broken into small molecules of some byproducts, including phenol [40]. Obviously, phenol is

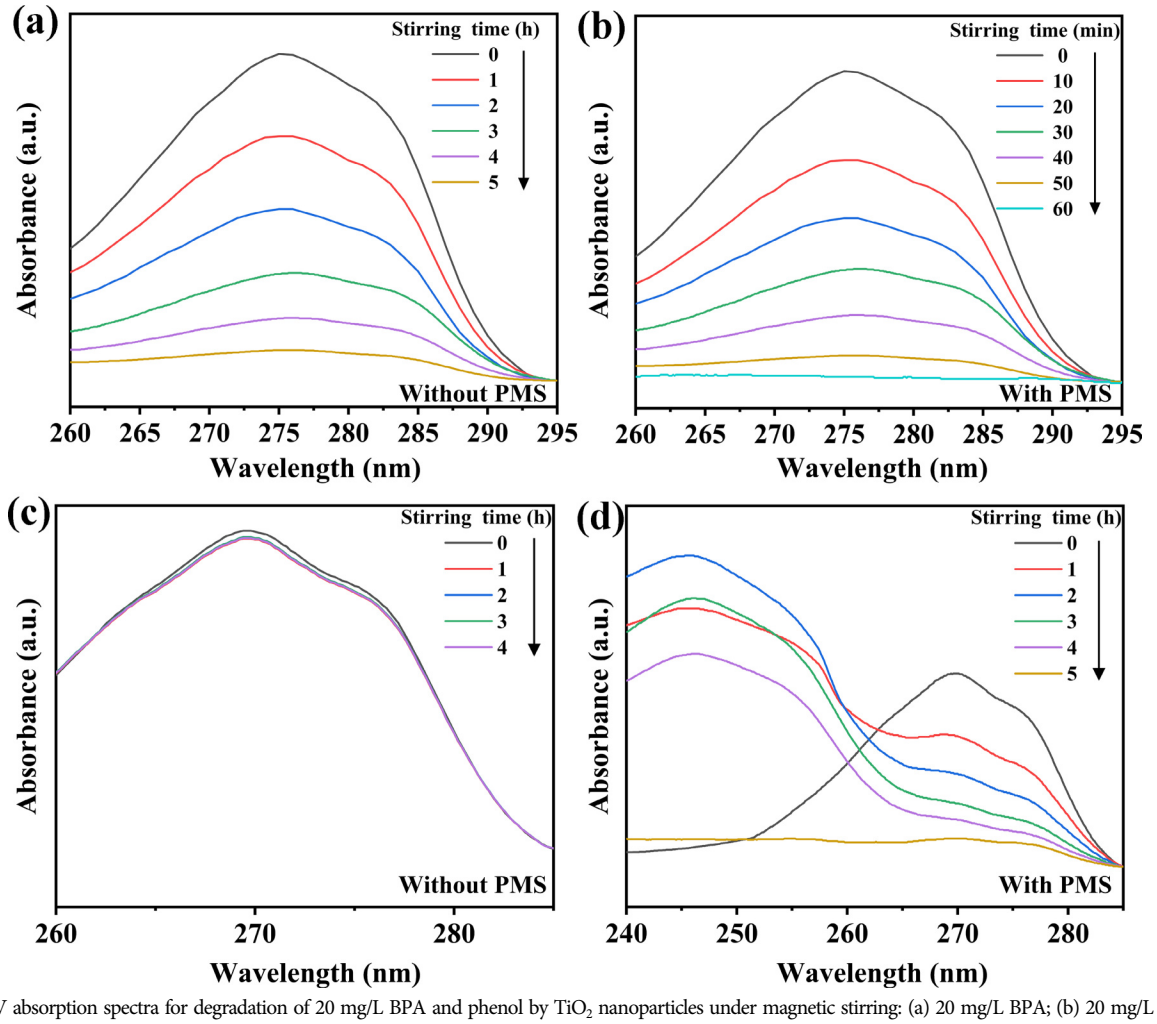

Fig. 3 UV absorption spectra for degradation of 20 mg/L BPA and phenol by TiO_2 nanoparticles under magnetic stirring: (a) 20 mg/L BPA; (b) 20 mg/L BPA and 200 mg/L PMS; (c) 20 mg/L phenol; (d) 20 mg/L phenol and 200 mg/L PMS.

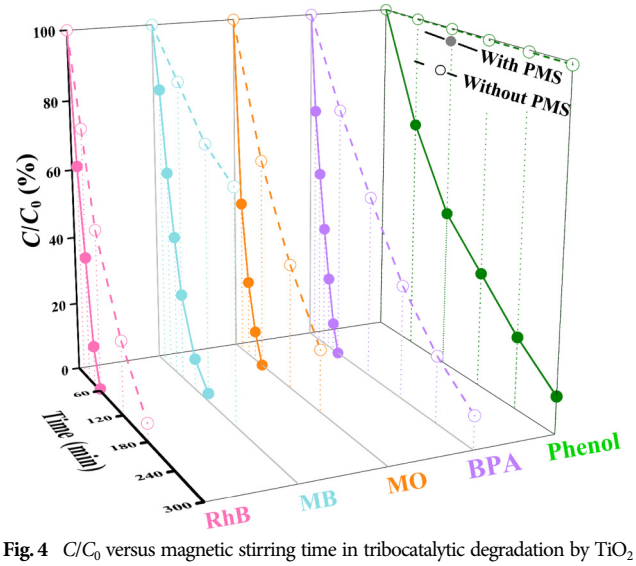

Fig. 4 C/C_0 versus magnetic stirring time in tribocatalytic degradation by TiO_2 nanoparticles for PMS-free and PMS-supplemented RhB, MB, MO, BPA, and phenol solutions.

relatively challenging to degrade through tribocatalysis. Fortunately, this transient peak disappeared after 5 h of magnetic stirring. Therefore, for all five kinds of organic pollutant solutions, PMS not only increased their tribocatalytic degradation speed by

Table 1 Pseudo-first-order rate constants for all pollutants with and without PMS in this study (Unit: min^{-1})

	RhB	MB	MO	BPA	Phenol
Without PMS	0.013	0.0026	0.0084	0.0069	0
With PMS	0.047	0.027	0.053	0.047	0.0064

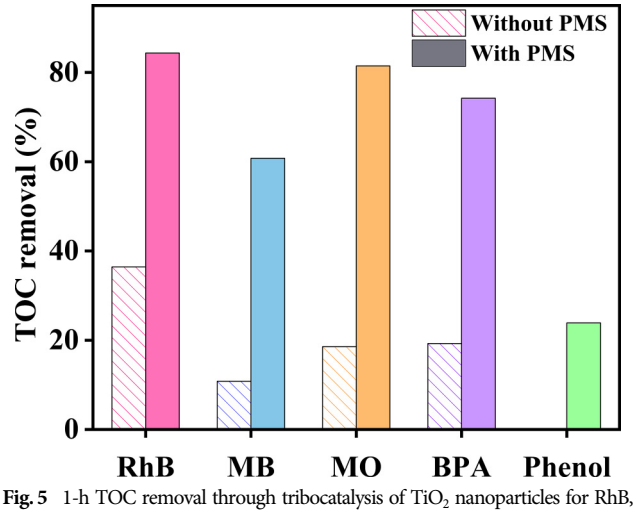

Fig. 5 1-h TOC removal through tribocatalysis of TiO_2 nanoparticles for RhB, MB, MO, BPA, and phenol solutions with and without PMS.

TiO_2 nanoparticles but also deepened their mineralization at a specific time point. These results thus expand the scope of pollutants amenable to tribocatalysis and lay a solid groundwork for subsequent mechanistic analysis and application development.

3.3 Control studies on effects of friction on systems of organic pollutant–PMS–TiO_2

To reveal the synergistic effect between tribocatalysis and PMS, a control study was conducted by replacing magnetic stirring in the experimental process with friction-free stirring. As shown in Fig. S2 in the ESM, an electric agitator was used for this purpose, which can stir solutions of organic dyes and PMS suspended with TiO_2 nanoparticles without forming any friction with the bottom of the beaker. Figure 6 shows the results obtained for 50 mg/L MB and 200 mg/L PMS suspended with TiO_2 nanoparticles treated through friction-free stirring. The curve measured for the MB solution before TiO_2 nanoparticles were added was marked as stirring time 0. As soon as TiO_2 nanoparticles were added, a ~12% drop in absorbance was observed, and then the absorbance decreased very slowly with time, indicating that the adsorption equilibrium was reached quickly. PMS was added at 30 min of stirring. It can be clearly seen that the absorbance decreased with time at a slightly higher speed after the PMS addition, and an additional ~13% drop in absorbance was observed at 90 min of stirring. This modest change associated with PMS addition forms a sharp contrast with that of PMS under magnetic stirring. The same results were also obtained for RhB and MO solutions, as shown in Fig. S3 in the ESM.

It is clear that under this friction-free stirring, the effect of PMS addition is negligible, and TiO_2 nanoparticles only show a small adsorption for the organic dyes. In other words, the surprising enhancement in the degradation of organic pollutants by PMS in this study is directly related to the friction that is responsible for the tribocatalysis of TiO_2 nanoparticles.

It is well-known that PMS can be directly activated through heat and UV irradiation. In studies on piezocatalytic activation of PMS/PDS, the activation of PMS/PDS by ultrasound in the absence of piezocatalysts has always been examined carefully [18–20]. Obviously, it is necessary to evaluate how PMS is activated through magnetic stirring in the absence of TiO_2 nanoparticles in this study. For this purpose, we conducted another control study on mixtures of organic pollutant-PMS treated through magnetic stirring in the dark, and the results are shown in Fig. 7. Noticeable degradation was observed for the RhB, MB, MO, and BPA solutions, while almost no detectable degradation was observed for the phenol solution. In fact, these results are quite similar to those obtained for TiO_2 nanoparticles without PMS, as shown in Fig. 4. Under magnetic stirring, on the one hand, the RhB, MB, MO, and BPA solutions can all be degraded by TiO_2 nanoparticles alone and by PMS alone, while on the other hand, with phenol as a well-known refractory organic pollutant, the phenol solution can only be degraded by the synergistic effect between TiO_2 nanoparticles and PMS under magnetic stirring. It can be concluded that while PMS can be directly activated to some extent through magnetic stirring alone, the greatly enhanced degradation obtained in this study must have resulted from a much more effective activation of PMS through the tribocatalysis of TiO_2 nanoparticles under magnetic stirring.

3.4 Mechanism for tribocatalytic activation of PMS by TiO_2 nanoparticles

The activation of PMS can be generally classified into two distinct ways: One is the direct homolysis of the peroxide bond in it through heating or ultraviolet irradiation; the other is the reaction with it by electrons generated through some catalysis processes [13]. Compared with homogeneous photocatalysis, heterogeneous photocatalysis has received increasing attention for PMS activation due to its capability to sustainably inject photogenerated electrons into the process in recent years [41]. A tribocatalytic mechanism based on the excitation of electron–hole pairs by mechanical energy absorbed through friction was first proposed for barium strontium titanate nanoparticles in 2019 [22]. Since then, this mechanism has been adopted for an increasing number of semiconductors as tribocatalysts [42]. For TiO_2 nanoparticles in this study, our results are consistent with such a mechanism, which can be specifically expressed as Reaction (1):

$$TiO_2 \xrightarrow{\text{Friction energy}} TiO_2 + e^- + h^+ \quad (1)$$

These tribo-generated charge carriers subsequently trigger the formation of free radicals in the ambient environment, as given by Reactions (2)–(4) [43]:

$$h^+ + H_2O \rightarrow \cdot OH + H^+ \quad (2)$$

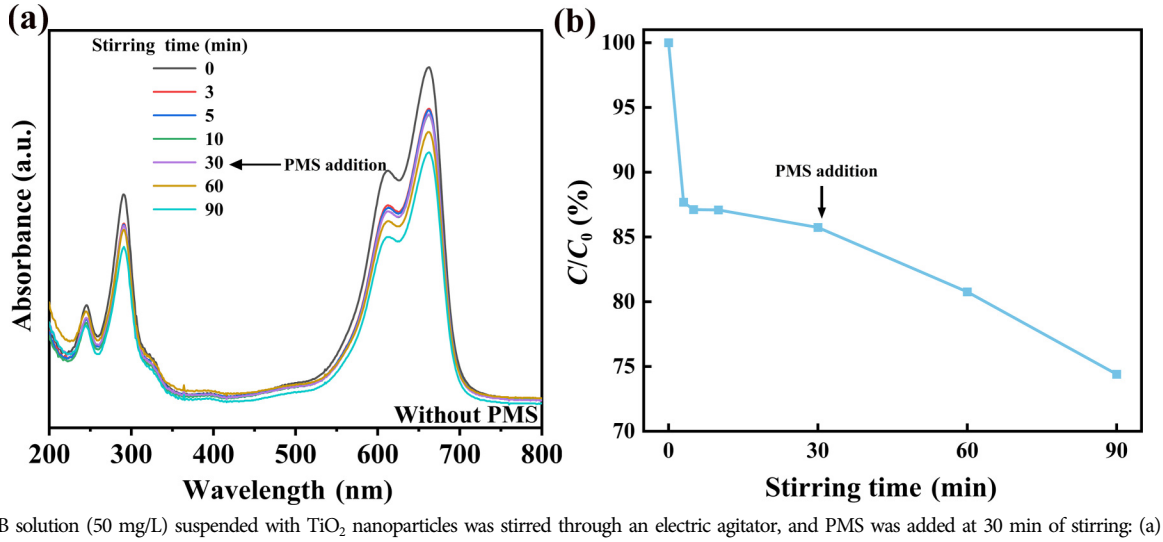

Fig. 6 MB solution (50 mg/L) suspended with TiO_2 nanoparticles was stirred through an electric agitator, and PMS was added at 30 min of stirring: (a) UV–Vis absorption spectra obtained at a series of stirring times; (b) corresponding curve of C/C_0 versus stirring time.

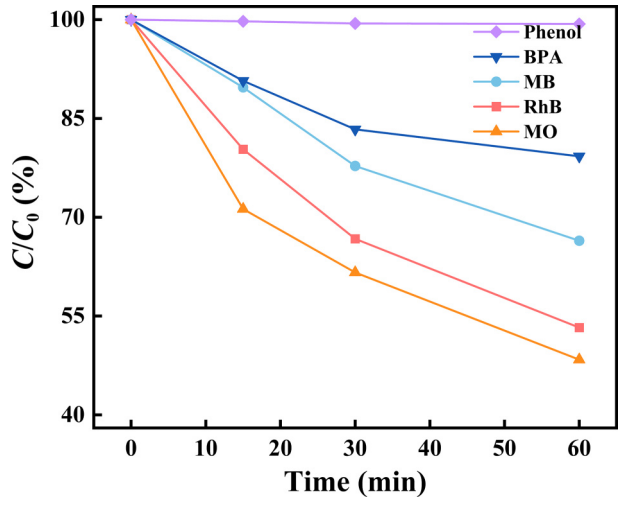

Fig. 7 C/C_0 versus magnetic stirring time for RhB, MB, MO, BPA, and phenol solutions with 200 mg/L PMS supplemented.

$$e^- + O_2 \rightarrow O_2 \cdot^- \quad (3)$$

$$O_2 \cdot^- + \cdot OH \rightarrow {}^1O_2 + OH^- \quad (4)$$

It is thus not surprising that ·OH, O_2·$^-$, and $^1O_2$ were observed in the PMS-free control experiments, as shown in Figs. 8(a)–8(c).

When PMS is present, electrons can activate it, as given in Reactions (5) and (6):

$$HSO_5^- + e^- \rightarrow \cdot OH + SO_4^{2-} \quad (5)$$

$$HSO_5^- + e^- \rightarrow OH^- + SO_4 \cdot^- \quad (6)$$

These two kinds of first-formed radicals not only react with pollutants but also lead to the formation of more kinds of reactive oxygen species, as shown in Reactions (7) and (8) [44]:

$$HSO_5^- + \cdot OH \rightarrow SO_5 \cdot^- + H_2O \quad (7)$$

$$HSO_5^- + SO_4 \cdot^- \rightarrow SO_5 \cdot^- + SO_4^{2-} + H^+ \quad (8)$$

Peroxymonosulfate radicals (SO_5·$^-$) easily undergo self-reaction to generate both sulfate radicals and singlet oxygen, as shown in Reaction (9) [45]:

$$2SO_5 \cdot^- \rightarrow 2SO_4 \cdot^- + {}^1O_2 \quad (9)$$

It is actually common for PMS activation that not only SO_4·$^-$ (DMPO–SO_4·$^-$) radicals are formed but also many other radicals are substantially increased, which can be clearly seen in Figs. 8(a)–8(c). Obviously, in the course of magnetic stirring applied to solutions suspended with TiO_2 nanoparticles, reactive species such

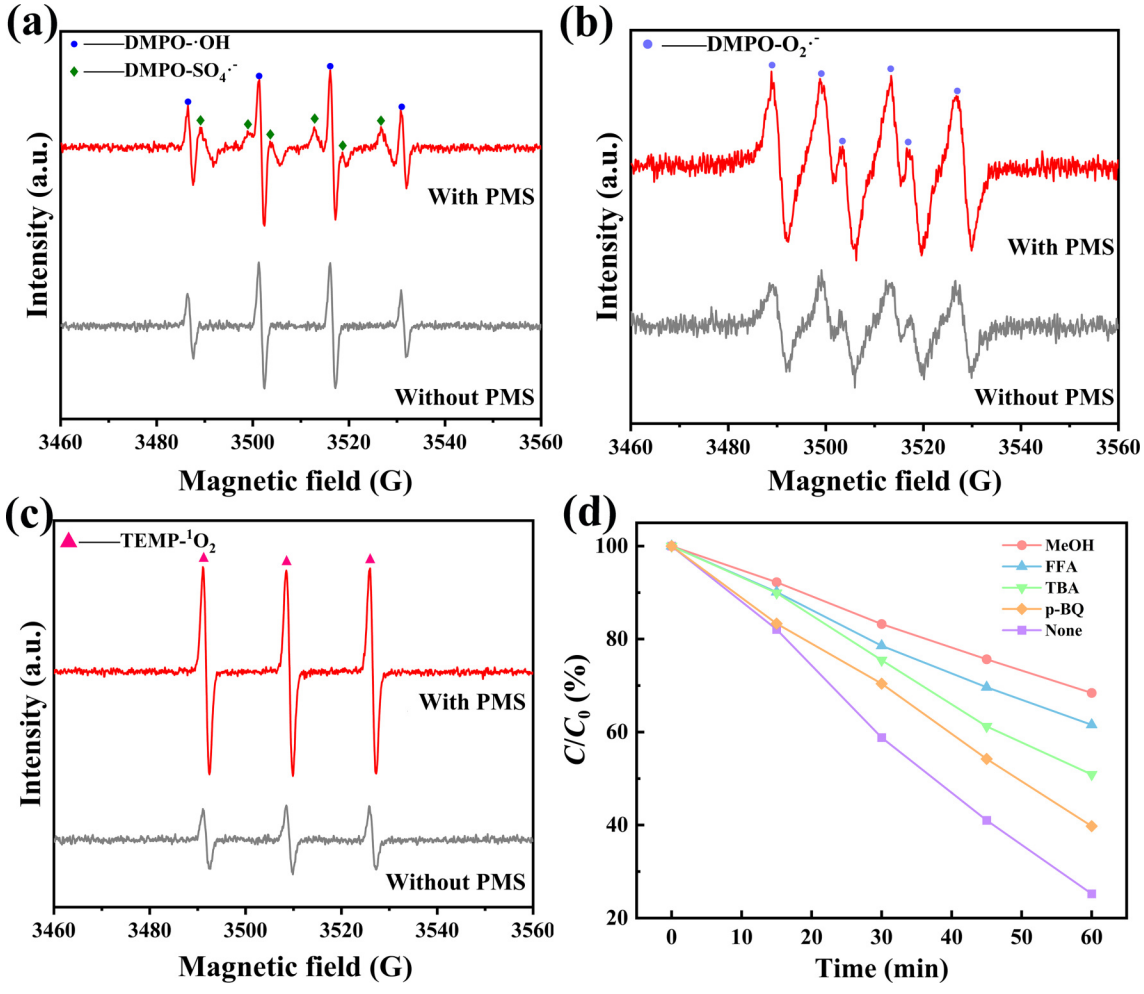

Fig. 8 EPR spectra measured for PMS-free and PMS-supplemented solutions suspended with TiO_2 nanoparticles and stimulated through magnetic stirring: (a) 10.0 mL deionized water with 0.05 mL DMPO as trapping agent; (b) 9.0 mL methanol with 0.05 mL DMPO as trapping agent; (c) 10.0 mL deionized water with 0.05 mL TEMP as trapping agent. (d) Effects of different scavengers on tribocatalytic degradation of 50 mg/L MB with 200 mg/L PMS by TiO_2 nanoparticles.

as ·OH, O_2·⁻, and $^1O_2$ can be readily generated, which should be responsible for the degradation of organic pollutants observed for TiO_2 nanoparticles. When PMS is present, not only ·OH, O_2·⁻, and $^1O_2$ are all substantially increased in amount, more radical species such as SO_4·⁻ are also formed, which should have resulted in the surprising enhancement in the degradation of organic pollutants observed for PMS addition.

As shown in Fig. 8(d), after 60 min of magnetic stirring, the original degradation efficiency of MB was 78.22%, while it decreased to 60.22%, 49.11%, 39.78%, and 31.58% with the addition of p-BQ, TBA, FFA, and MeOH, respectively. Among all these quenchers, MeOH and FFA exhibited the most pronounced inhibitory effects. It is worth noting that while MeOH quenches both SO_4·⁻ and ·OH radicals, FFA quenches the nonradical $^1O_2$ alone. Obviously, both radical and nonradical pathways contribute to the degradation process [45–47], confirming the synergistic effect between TiO_2 nanoparticles and PMS under magnetic stirring.

Generally, this tribocatalytic activation process of PMS by TiO_2 nanoparticles is quite similar to the photocatalytic activation of PMS reported in Ref. [48]. Namely, electron–hole pairs are first excited in TiO_2 nanoparticles, which subsequently trigger the formation of radicals in the ambient environment and activate PMS to generate more radicals when present, as schematically shown in Fig. 9. These charge carriers and radicals synergistically contribute to the degradation of organic pollutants, which can be formally expressed as Reaction (10):

$$e^-/h^+/\cdot OH/SO_4\cdot^-/O_2\cdot^-/^1O_2 + \text{Organics} \rightarrow CO_2 + H_2O \quad (10)$$

For SO_4·⁻, its one-electron redox potential (2.5–3.1 V vs NHE) is substantially higher than that of ·OH (1.9–2.7 V), and it exhibits a lifetime of tens of microseconds, far exceeding the nanosecond-scale lifetime of ·OH. Additionally, SO_4·⁻ retains strong reactivity across a broad pH range, whereas ·OH is readily quenched under neutral to alkaline conditions [49,50]. Furthermore, with a higher redox potential than molecular oxygen, PMS acts as a superior electron sink, competitively capturing electrons and thereby suppressing e^-/h^+ recombination [48]. All these features should have resulted in a great enhancement in tribocatalytic degradation of organic pollutants by TiO_2 nanoparticles after PMS is supplemented.

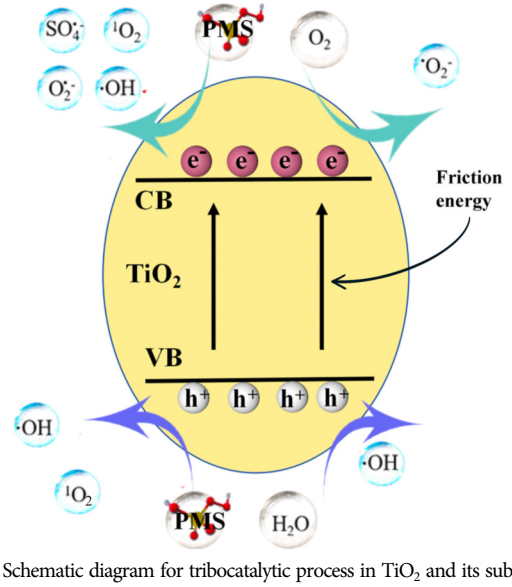

Fig. 9 Schematic diagram for tribocatalytic process in TiO_2 and its subsequent activation of PMS.

While numerous investigations have been conducted to activate PDS/PMS through homogeneous photocatalysis [51], heterogeneous photocatalysis [52], and piezocatalysis [53], to our knowledge, this work has successfully utilized mechanical energy for the first time to activate PMS via tribocatalysis for the degradation of organic pollutants. It is highly encouraging that in this first study on the combination of tribocatalysis and PMS, 50 mg/L RhB, MB, and MO, as well as 20 mg/L BPA and phenol solutions, were all rather thoroughly degraded in relatively short periods of time through low-frequency magnetic stirring. Beyond demonstrating these specific performances, this study actually broadens the paradigm of PMS activation and suggests a new avenue for advanced oxidation processes.

As pointed out in a previous study [54], the power of magnetic stirring with a PTFE magnetic disk rotated at 400 r/min was below 10 W. This suggests that friction formed through rotation is very effective in converting mechanical energy into chemical energy for the tribocatalytic degradation of organic pollutants. To enlarge the scale, much larger disks can be readily driven to rotate through motors to input low-frequency mechanical energy for tribocatalysis. With the enhancement of tribocatalysis by PMS shown in this study, we anticipate that the combination of PMS/PDS and tribocatalysis will provide a viable, sustainable route toward the application of PMS/PDS.

4 Conclusions

The combination of PMS and tribocatalysis was first investigated by adding PMS to solutions of organic pollutants subjected to tribocatalytic degradation by TiO_2 nanoparticles. For five representative organic pollutants, their tribocatalytic degradation was greatly enhanced with the addition of 200 mg/L PMS, and rather thorough degradation was realized in a short period of time: 50 mg/L RhB was degraded by 100% in 1 h, 50 mg/L MB was degraded by 97.7% in 2 h, 50 mg/L MO was degraded by 99.9% in 1 h, 20 mg/L BPA was degraded by 99.8% in 1 h, and 20 mg/L phenol was degraded by 90.0% in 5 h. At the same time, their total organic carbon removals were substantially improved. According to electron paramagnetic resonance spectroscopy analyses, PMS was activated by TiO_2 nanoparticles under magnetic stirring to generate SO_4·⁻ and increase the amount of ·OH, O_2·⁻, and $^1O_2$. These findings demonstrate a tribocatalytic activation of PMS input with low-frequency mechanical energy of magnetic stirring, which suggests a powerful green technology for the applications of PMS/PDS.

Acknowledgements

This work was partially supported by the National Natural Science Foundation of China (No. U24A20203) and Jiangsu Engineering Research Center of New Materials for Adsorptive Separation in Chemical Industry and Environmental Treatment, Suzhou, 215123, China (No. SDGC2424).

Availability of data and materials

The data that support the findings of this study are available from the corresponding author upon reasonable request.

Competing interests

The authors have no competing interests to declare that are relevant to the content of this article.

Electronic Supplementary Material

Supplementary material is available in the online version of this article at https://doi.org/10.26599/JAC.2025.9221237.

References

[1] Lin JY, Ye WY, Xie M, *et al.* Environmental impacts and remediation of dye-containing wastewater. *Nat Rev Earth Env* 2023, **4**: 785–803.

[2] Rokni L, Rezaei M, Rafieizonooz M, *et al.* Effect of persistent organic pollutants on human health in south Korea: A review of the reported diseases. *Sustainability* 2023, **15**: 10851.

[3] Razavi L, Raissi H, Hashemzehi O, *et al.* Significantly enhanced performance for phenol compounds removal by MOF-5 nano-composite via its surface modification. *npj Clean Water* 2024, **7**: 44.

[4] Rathi BS, Kumar PS, Show PL. A review on effective removal of emerging contaminants from aquatic systems: Current trends and scope for further research. *J Hazard Mater* 2021, **409**: 124413.

[5] Brillas E, Martínez-Huitle CA. Decontamination of wastewaters containing synthetic organic dyes by electrochemical methods. An updated review. *Appl Catal B—Environ* 2015, **166–167**: 603–643.

[6] Deng Y, Zhao RZ. Advanced oxidation processes (AOPs) in wastewater treatment. *Curr Pollut Rep* 2015, **1**: 167–176.

[7] Parvulescu VI, Epron F, Garcia H, *et al.* Recent progress and prospects in catalytic water treatment. *Chem Rev* 2022, **122**: 2981–3121.

[8] Lim S, Shi JL, von Gunten U, *et al.* Ozonation of organic compounds in water and wastewater: A critical review. *Water Res* 2022, **213**: 118053.

[9] Hübner U, Spahr S, Lutze H, *et al.* Advanced oxidation processes for water and wastewater treatment–Guidance for systematic future research. *Heliyon* 2024, **10**: 30402.

[10] Cao ZF, Yu XM, Zheng YZ, *et al.* Micropollutant abatement by the UV/chloramine process in potable water reuse: A review. *J Hazard Mater* 2022, **424**: 127341.

[11] Marron EL, Mitch WA, von Gunten U, *et al.* A tale of two treatments: The multiple barrier approach to removing chemical contaminants during potable water reuse. *Acc Chem Res* 2019, **52**: 615–622.

[12] Miklos DB, Remy C, Jekel M, *et al.* Evaluation of advanced oxidation processes for water and wastewater treatment–A critical review. *Water Res* 2018, **139**: 118–131.

[13] Xia XH, Zhu FY, Li JJ, *et al.* A review study on sulfate-radical-based advanced oxidation processes for domestic/industrial wastewater treatment: Degradation, efficiency, and mechanism. *Front Chem* 2020, **8**: 592056.

[14] Xie ZH, He CS, Zhou HY, *et al.* Effects of molecular structure on organic contaminants' degradation efficiency and dominant ROS in the advanced oxidation process with multiple ROS. *Environ Sci Technol* 2022, **56**: 8784–8795.

[15] Lee J, von Gunten U, Kim JH. Persulfate-based advanced oxidation: Critical assessment of opportunities and roadblocks. *Environ Sci Technol* 2020, **54**: 3064–3081.

[16] Guerra-Rodríguez S, Rodríguez E, Singh DN, *et al.* Assessment of sulfate radical-based advanced oxidation processes for water and wastewater treatment: A review. *Water* 2018, **10**: 1828.

[17] Nie G, Xiao L, Bi JX, *et al.* New insight to piezocatalytic peroxymonosulfate activation: The critical role of dissolved oxygen in mediating radical and nonradical pathways. *Appl Catal B—Environ* 2022, **315**: 121584.

[18] Lan SY, Chen YX, Zeng LX, *et al.* Piezo-activation of peroxymonosulfate for benzothiazole removal in water. *J Hazard Mater* 2020, **393**: 122448.

[19] Chen YX, Lan SY, Zhu MS. Construction of piezoelectric $BaTiO_3$/MoS_2 heterojunction for boosting piezo-activation of peroxymonosulfate. *Chinese Chem Lett* 2021, **32**: 2052–2056.

[20] Zhang MX, Tao HC, Zhai CY, *et al.* Twin-brush ZnO mesocrystal for the piezo-activation of peroxymonosulfate to remove ibuprofen in water: Performance and mechanism. *Appl Catal B—Environ* 2023, **326**: 122399.

[21] Urán-Duque L, Saldarriaga-Molina JC, Rubio-Clemente A. Advanced oxidation processes based on sulfate radicals for wastewater treatment: Research trends. *Water* 2021, **13**: 2445.

[22] Li PC, Wu J, Wu Z, *et al.* Strong tribocatalytic dye decomposition through utilizing triboelectric energy of barium strontium titanate nanoparticles. *Nano Energy* 2019, **63**: 103832.

[23] Jia XC, Wang HB, Lei H, *et al.* Boosting tribo-catalytic conversion of H_2O and CO_2 by Co_3O_4 nanoparticles through metallic coatings in reactors. *J Adv Ceram* 2023, **12**: 1833–1843.

[24] Jin ZH, Su B, Wu S, *et al.* Tribocatalytic recycling of lithium-ion batteries. *J Adv Ceram* 2025, **14**: 9221121.

[25] Mao CY, Guo ZY, Chen WP. Coating disk-shaped materials on the bottoms of vessels: A convenient while marvelous practice for tribocatalysis. *Surf Interfaces* 2025, **60**: 106106.

[26] Emmanuel SS, Adesibikan AA. Harvesting surface (interfacial) energy for tribocatalytic degradation of hazardous dye pollutants using nanostructured materials: A review. *J Chin Chem Soc-Taip* 2024, **71**: 944–977.

[27] Zhu MZ, Zhou ZR, Gu YH, *et al.* Powerful tribocatalytic degradation of methyl orange solutions with concentrations as high as 100 mg/L by $BaTiO_3$ nanoparticles. *Nanomaterials* 2025, **15**: 1135.

[28] Chen FT, Liu Z, Liu Y, *et al.* Enhanced adsorption and photocatalytic degradation of high-concentration methylene blue on Ag_2O-modified TiO_2-based nanosheet. *Chem Eng J* 2013, **221**: 283–291.

[29] Mao CY, Zhang YC, Lei H, *et al.* Boosting tribo-catalytic degradation of organic pollutants by $BaTiO_3$ nanoparticles through metallic coatings. *Appl Surf Sci* 2024, **663**: 160172.

[30] Cui XD, Li PC, Lei H, *et al.* Greatly enhanced tribocatalytic degradation of organic pollutants by TiO_2 nanoparticles through efficiently harvesting mechanical energy. *Sep Purif Technol* 2022, **289**: 120814.

[31] Shi YF, Chen JB, Xiao SZ, *et al.* Revisiting the mineralization of organic contaminants in advanced oxidation processes. *ACS EST Water* 2023, **3**: 3449–3451.

[32] Mao CY, Lei H, Guo ZY, *et al.* Exceptional tribo-catalytic degradation of concentrated methyl orange and methylene blue solutions by DXN-RT30 TiO_2 nanoparticles. *Ceram Int* 2024, **50**: 4737–4745.

[33] Gu YH, Li YE, Wang KL, *et al.* Greatly enhanced tribocatalytic purification of concentrated dye wastewater by TiO_2 nanoparticles through Ti and Al_2O_3 coatings. *Colloid Interfac Sci* 2025, **67**: 100851.

[34] Zhou ZR, Luo RQ, Mao CY, *et al.* Contrasting tribocatalytic degradations of organic dyes by two different commercial silicon powders. *J Adv Dielectr* 2025, **15**: 2450025.

[35] Che JL, Gao YH, Wu Z, *et al.* Review on tribocatalysis through harvesting friction energy for mechanically-driven dye decomposition. *J Alloy Compd* 2024, **1002**: 175413.

[36] Ahmaruzzaman M, Mishra SR, Gadore V, *et al.* Phenolic compounds in water: From toxicity and source to sustainable solutions–An integrated review of removal methods, advanced technologies, cost analysis, and future prospects. *J Environ Chem Eng* 2024, **12**: 112964.

[37] Razia S, Hadibarata T, Lau SY. A review on biodegradation of Bisphenol A (BPA) with bacteria and fungi under laboratory conditions. *Int Biodeter Biodegr* 2024, **195**: 105893.

[38] Saputera WH, Putrie AS, Esmailpour AA, *et al.* Technology advances in phenol removals: Current progress and future perspectives. *Catalysts* 2021, **11**: 998.

[39] Olmez-Hanci T, Arslan-Alaton I. Comparison of sulfate and hydroxyl radical based advanced oxidation of phenol. *Chem Eng J* 2013, **224**: 10–16.

[40] Cui XD, Guo ZY, Lei H, *et al.* Tribo-catalytic degradation of methyl orange solutions enhanced by silicon single crystals. *Coatings* 2023, **13**: 1804.

[41] Shi H, He Y, Li YB, *et al.* Unraveling the synergy mechanism between photocatalysis and peroxymonosulfate activation on a Co/Fe bimetal-doped carbon nitride. *ACS Catal* 2023, **13**: 8973–8986.

[42] Li XN, Tong WS, Shi J, *et al.* Tribocatalysis mechanisms: Electron transfer and transition. *J Mater Chem A* 2023, **11**: 4458–4472.

[43] Lim HJ, Kim DJ, Rigby K, *et al.* Peroxymonosulfate-based

electrochemical advanced oxidation: Complication by oxygen reduction reaction. *Environ Sci Technol* 2023, **57**: 19054–19063.
[44] Tang WJ, Wang ZJ, Guo S, *et al*. Efficient generation of $^1O_2$ by activating peroxymonosulfate on graphitic carbon nanoribbons for water remediation. *npj Clean Water* 2024, **7**: 92.
[45] Jia Y, Chen YY, Xue YH, *et al*. Efficient activation of peroxymonosulfate by Mn single-atom: Critical role of Mn–N_4 coordination for generating singlet oxygen. *Sep Purif Technol* 2024, **335**: 126129.
[46] Chen TT, Zhang GB, Sun HW, *et al*. Robust Fe–N_4–C_6O_2 single atom sites for efficient PMS activation and enhanced Fe^{IV} = O reactivity. *Nat Commun* 2025, **16**: 2402.
[47] Sun YL, Yang L, Feng HY, *et al*. Synthesize and application of high entropy single atom catalyst for PMS activation: Performance and mechanism. *Sep Purif Technol* 2026, **380**: 135215.
[48] Deng J, Chen WG, Wu F, *et al*. Peroxymonosulfate activation by Ni–Fe (hydr)oxides through radical and nonradical pathways for efficient trichloroethylene degradation. *Sep Purif Technol* 2023, **325**: 124675.
[49] Feng S, Xie TP, Wang JK, *et al*. Photocatalytic activation of PMS over magnetic heterojunction photocatalyst $SrTiO_3/BaFe_{12}O_{19}$ for tetracycline ultrafast degradation. *Chem Eng J* 2023, **470**: 143900.
[50] Zhao XY, Zhang ZH. Heterogeneous peroxymonosulfate-based advanced oxidation mechanisms: New wine in old bottles. *Environ Sci Technol* 2025, **59**: 5913–5924.
[51] Xiao S, Cheng M, Zhong H, *et al*. Iron-mediated activation of persulfate and peroxymonosulfate in both homogeneous and heterogeneous ways: A review. *Chem Eng J* 2020, **384**: 123265.
[52] Wang AW, Du M, Ni JX, *et al*. Enhanced and synergistic catalytic activation by photoexcitation driven S-scheme heterojunction hydrogel interface electric field. *Nat Commun* 2023, **14**: 6733.
[53] Sankari Jeyabalan S, Sudhir Ekande O, Mainali B, *et al*. A systematic review of recent advances in piezocatalysis—Synergetic heterojunctions for organic pollutants removal, immobilization, and scope of machine learning techniques. *Chem Eng J* 2024, **498**: 155086.
[54] Xu X, Mao CY, Ke SH, *et al*. Greatly enhanced tribocatalytic degradation of organic dyes by Fe_2O_3 nanoparticles through Ti and Al_2O_3 coatings. *J Mater Sci* 2025, **60**: 7333–7342.